Sliding Mode Formation Control for Multiple Hypersonic Glide Vehicles

Dongdong Yao[1,*], Yandong Hu[2], Dawei Liu[3] and Qunli Xia[1]
[1] *School of Aerospace, Beijing Institute of Technology, Beijing, China*
[2] *Zhengzhou University of Aeronautics, Zhengzhou, China*
[3] *China Research Development Academy of Machinery, Beijing, China*

Keywords: Hypersonic Glide Vehicle, Formation Controller, Sliding Mode Control, State Observer, Sign of Bank Angle.

Abstract: Aiming at the formation flying problem multiple hypersonic gliding vehicles, a formation controller design method based on sliding mode control theory is proposed. Firstly, according to the vehicle motion model and the multi-body "leader-follower" motion model, the trajectory of the leader and the state equation of the follower are obtained. Based on the sliding mode control theory, a formation controller is designed to maintain the relative position between the follower and the leader in terms of altitude and speed. The extended state observer is designed to eliminate formation modeling errors and flight process errors. On this basis, the control variable is transformed from acceleration to attack angle and bank angle. According to the lateral relative position and heading angle direction, the sign change logic of the bank angle is designed to ensure that the lateral relative position can meet the formation distance requirements. Simulation results show that the proposed control method can achieve the desired multi-hypersonic vehicle formation flying.

1 INTRODUCTION

Hypersonic glide vehicle has become the focus of research in many countries because of its high speed, high precision and long range (ZHAO, 2014). Facing the complex battlefield environment and diverse combat tasks, with the improvement of vehicle performance, multiple hypersonic vehicles can improve the communication and detection ability during glide by flying in formation, and is conducive to the realization of coordinated attack on the target during the terminal guidance period. Therefore, it is important to study the formation control method of multiple hypersonic glide vehicles (GUO, 2022; SHUI, 2020).

Hypersonic glide vehicle has the characteristics of strong nonlinear model, severe flight environment, wide flight space and strict flight constraints. Its only control force is aerodynamic, so accurate formation control of hypersonic vehicles is very complicated and difficult to achieve (An, 2022). Therefore, when considering the formation space configuration, it is not necessary to keep an accurate space configuration of multiple aircraft, but only need to maintain the relative position in a certain space to form an "inaccurate formation", so as to ensure that the aircrafts can realize the communication, detection, middle and terminal guidance transition and other functions during the flight.

The cooperative formation control of hypersonic glide vehicles can be based on three methods (WANG, 2019). The first is based on the cooperative trajectory planning of multiple aircraft, and obtains the trajectory of each aircraft by setting various constraints of the aircraft (CHU, 2017; YU, 2020; GAO, 2022). The second is based on the formation controller, which is usually based on the "leader-follower" formation model. The formation controller is designed to keep the following aircraft (hereinafter referred to as "follower") in relative space position (ZHANG, 2021; ZHANG, 2021; WEI, 2022). The third is based on the distributed consensus algorithm, and according to the communication topology, the consistency control law is designed to realize the formation flight of multiple aircraft (Wei, 2021; Zhao, 2017; LI, 2020). Among them, the first method can fully consider the flight capability of the aircraft, but it usually establishes the cooperative control law through the flight time, and the cooperative trajectory planning method through the formation space configuration

Yao, D., Hu, Y., Liu, D. and Xia, Q.
Sliding Mode Formation Control for Multiple Hypersonic Glide Vehicles.
DOI: 10.5220/0012150900003562
In *Proceedings of the 1st International Conference on Data Processing, Control and Simulation (ICDPCS 2023)*, pages 133-140
ISBN: 978-989-758-675-0

still needs further research. The second method is easier and more efficient to realize formation and maintenance, but the formation members are highly dependent on the information of the leading aircraft (hereinafter referred to as "leader"), which is easy to be interfered with. The third method can also quickly form and maintain formation, and is less affected by a single aircraft, but it puts forward higher requirements on the ability of aircraft to communicate and process information. In addition, due to the lack of thrust and the under-saturation and strong coupling characteristics of the gliding vehicle (WANG, 2018), the three-axis's acceleration cannot be projected directly into the aerodynamic force, which makes it difficult to deal with the control variable obtained by the latter two methods above.

Based on the above research, this paper takes the hypersonic glide vehicle as the research object and designs a sliding mode formation controller based on the "leader-follower" formation model to ensure that multiple vehicles maintain relative configuration within a certain range during flight. Firstly, according to the aircraft motion model and the "leader-follower" formation model, the leader trajectory is given and the follower state equation is obtained. Then, according to the sliding mode control theory, a formation controller with extended state observer (ESO) is designed to satisfy the formation requirements of multiple aircraft. Considering that attack angle and bank angle are the actual control variables, the calculation method of the attack angle and the sign change method of the bank angle are designed so that the horizontal direction of aircraft can meet the relative distance constraints. Simulation results show the effectiveness of the method.

2 HYPERSONIC VEHICLE MODEL DESCRIPTION

The motion model of the aircraft refers to the literature (Lu, 2014), and there is a three-degree-of-freedom motion equation in the half-velocity coordinate system, as shown in fig.1.

where, r is the distance between the vehicle and the center of the earth, λ and φ denote latitude and longitude respectively, v is the velocity of the vehicle, θ and ψ denote flight path angle and azimuth angle respectively, m is for mass, σ is the bank angle, g is the acceleration of gravity. D and L represent drag and lift, whose calculation formula is shown as fig. 2.

$$\begin{cases} \dot{r} = v\sin\theta \\ \dot{\lambda} = \dfrac{v\cos\theta\sin\psi}{r\cos\phi} \\ \dot{\phi} = \dfrac{v\cos\theta\cos\psi}{r} \\ \dot{v} = -\dfrac{1}{m}D - g\sin\theta \\ \dot{\theta} = \dfrac{L\cos\sigma}{mv} - \dfrac{g\cos\theta}{v} + \dfrac{v\cos\theta}{r} \\ \dot{\psi} = -\dfrac{L\sin\sigma}{mv\cos\theta} - \dfrac{v\tan\phi\cos\theta\sin\psi}{r} \end{cases} \tag{1}$$

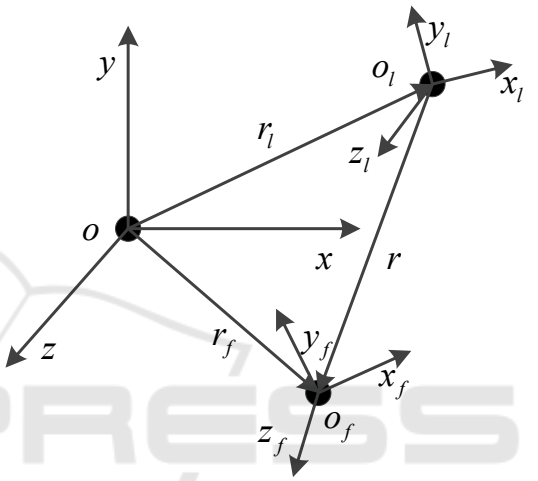

Figure 1: Relative motion relation of the leader and follower.

$$\begin{cases} L = qSC_L \\ D = qSC_D \end{cases} \tag{2}$$

where, q is the dynamic pressure, S is the aerodynamic reference area, C_L and C_D represent lift coefficient and drag coefficient.

Considering the dynamic pressure, heat flux density and overload constraints of the leader, there is

$$\begin{cases} q \le q_{max} \\ \dot{Q} \le \dot{Q}_{max} \\ n < n_{max} \end{cases} \tag{3}$$

where, $\dot{Q}$ is the heat flux density, n is the overload, the subscript *max* indicates the maximum value.

The formation model is established according to the reference (Amer, 2020), as shown in fig.1.

Taking the leader trajectory coordinate system as the reference system, the relative motion equations for the leader and follower are give:

$$\begin{cases} \dot{x} = \cos\theta_l\cos\theta_f\cos\left(\psi_l-\psi_f\right)v_f + \sin\theta_l\sin\theta_f v_f + \dot{\theta}_l y - \cos\theta_l\dot{\psi}_l z - v_l \\ \dot{y} = -\sin\theta_l\cos\theta_l\cos\left(\psi_l-\psi_f\right)v_f + \cos\theta_l\sin\theta_f v_f - \dot{\theta}_l x + \sin\theta_l\dot{\psi}_l z \\ \dot{z} = \cos\theta_f\sin\left(\psi_l-\psi_f\right)v_f + \cos\theta_l\dot{\psi}_l x - \sin\theta_l\dot{\psi}_l y \\ \dot{v}_f = a_x \\ \dot{\theta}_f = \dfrac{a_y}{v_f} \\ \dot{\psi}_f = -\dfrac{a_z}{v_f\cos\theta_f} \end{cases} \tag{4}$$

$$\begin{cases} \dot{x} = \cos\left(\psi_l-\psi_f\right)v_f + \theta_l\theta_f v_f + \dot{\theta}_l y - \dot{\psi}_l z + d_x \\ \dot{y} = -\theta_l\cos\left(\psi_l-\psi_f\right)v_f + \theta_f v_f - \dot{\theta}_l x + \theta_l\dot{\psi}_l z + d_y \\ \dot{z} = \sin\left(\psi_l-\psi_f\right)v_f + \dot{\psi}_l x - \theta_l\dot{\psi}_l y + d_z \\ \dot{v}_f = a_x \\ \dot{\theta}_f = \dfrac{a_y}{v_f} \\ \dot{\psi}_f = -\dfrac{a_z}{v_f\cos\theta_f} \end{cases} \tag{5}$$

where, the subscript l indicates the states of the leader, the subscript f indicates the states of followers, x, y and z represent three-axis's relative position of followers, a_x, a_y and a_z are three-axis's acceleration.

For the formation model shown in equation (4), since the relative position equation of the follower is established in the leader trajectory coordinate system, and the earth curvature is not taken into consideration, the reference inertial coordinate system of the leader and the followers is the ground coordinate system (NUE coordinate system) during the coordinate system transformation. However, when the curvature of the earth is considered, the ground coordinate system of the two will no longer coincide. At this time, the relative position obtained ccording to equation (3) will result in modeling errors caused by curvature. When two vehicles are 10km apart, the error value is about 8m, when the they are 100km apart, the error value is about 0.8km. It can be seen that if the relative position of the leader and follower is less than 100km, the relative error is less than 1%, but as the distance increases, the absolute error also increases, and the error needs to be properly processed according to the requirements.

In the simulation of most literatures (Brian, 2021; Wang, 2018; Wang, 2017), the absolute value of flight path angle is no more than 10°, so it can be simplified as follows: $\sin\theta = \theta$, $\cos\theta = 1$. Meanwhile, considering the modeling and process errors d_x, d_y and d_z, equation (3) can be simplified as equation (5)

3 DESIGN OF SLIDING MODE FORMATION CONTROLLER

According to reference (LI, 2021), keeping a specific space configuration during the flight of multiple hypersonic vehicles can improve the detection ability of the group. In this paper, the formation space configuration of multi-vehicle is "one-line". Due to the constraint of aircraft control ability, the distance between two aircraft in Z-axis direction should be given within a certain range. The minimum distance R_{min} is given according to the safe distance between the two aircraft, and the maximum distance R_{max} is given according to the communication ability.

3.1 Sliding Mode Controller Design

According to equation (5), the state equation of

aircraft can be written as equation (6). Since the distance in the z direction is controlled by the bank angle symbol, it only needs to design the sliding mode surface that controls the state in the x and y directions.

$$\begin{cases}\dot{X}_1 = AX_1 + BX_2 + F + D \\ \dot{X}_2 = GU\end{cases} \tag{6}$$

$$X_1 = \begin{bmatrix} x & y \end{bmatrix}^T \quad X_2 = \begin{bmatrix} v_f & \theta_f v_f \end{bmatrix}^T \quad U = \begin{bmatrix} a_x & a_y \end{bmatrix}^T$$

$$A = \begin{bmatrix} 0 & \dot{\theta}_l \\ -\dot{\theta}_l & 1 \end{bmatrix} \qquad B = \begin{bmatrix} cos\left(\psi_l - \psi_f\right) & \theta_l \\ -cos\left(\psi_l - \psi_f\right)\theta_l & 1 \end{bmatrix}$$

$$F = \begin{bmatrix} -v_l - \dot{\psi}_l z \\ \theta_l \dot{\psi}_l z \end{bmatrix} \qquad G = \begin{bmatrix} 1 & 0 \\ \theta_f & 1 \end{bmatrix}$$

$$D = \begin{bmatrix} d_x & d_y \end{bmatrix}$$

According to the design principle of sliding mode control (Li, 2005), the function of sliding mode and the approach law are taken

$$\begin{cases} s = ce_1 + e_2 \\ \dot{s} = -\varepsilon \mathrm{sgn}\left(s\right) - ks \quad \varepsilon > 0, k > 0 \end{cases}$$

$$\begin{aligned} e_1 &= X_{1d} - X_1 \\ e_2 &= X_{2d} - X_2 \end{aligned} \tag{7}$$

where, X_{1d} and X_{2d} are the expected values of X_1 and X_2. For X_{2d}. Using the backstepping method, X_{2d} can be expressed as

$$X_{2d} = B^{-1}\left(-k_1 e_1 - AX_1 - F - D\right) \tag{8}$$

In order to track and keep the relative position of the follower, according to equation (7), there is

$$\begin{aligned} &s = ce_1 + e_2 \\ &e_1 = X_{1d} - X_1 \\ &e_2 = X_{2d} - X_2 \\ &c\left(\dot{X}_{1d} - \dot{X}_1\right) + \left(\dot{X}_{2d} - \dot{X}_2\right) = -\varepsilon \mathrm{sgn}\left(s\right) - ks \end{aligned} \tag{9}$$

The control law is obtained by taking equation (6) into equation (8), show as in equation (10)

$$U = G^{-1}\begin{bmatrix} c\left(\dot{X}_{1d} - AX_1 - BX_2 - F - D\right) + \\ \dot{X}_{2d} + \varepsilon\, sgn\left(s\right) + ks \end{bmatrix} \tag{10}$$

The design of the sliding mode surface and the reaching law above can ensure $s\dot{s} \le 0$, that is, Lyapunov function $V = s^2/2$ is positive definite and its derivative is negative definite. The system can stabilize on the sliding mode surface after reaching it, that is, the error tends to zero.

3.2 Extended State Observer Design

According to reference (Li, 2005), an extended state observer is designed to estimate the bounded composite disturbance D.

First define the expanded state X_{1e}, assuming $\dot{D} = \upsilon$, considering the first formula in equation (6), the state equation can be written as

$$\begin{cases}\dot{X}_1 = AX_1 + BX_2 + F + X_{1e} \\ \dot{X}_{1e} = \upsilon\end{cases} \tag{11}$$

The ESO is used to estimate X_1 and X_{1e}, and the calculation formula is

$$\begin{cases} E_1 = Z_{11} - X_1 \\ \dot{Z}_{11} = AX_1 + BX_2 + F + Z_{12} - \beta_{11} E_1 \\ \dot{Z}_{12} = -\beta_{12}\, fal\left(E_1, \alpha, \delta\right) \end{cases} \tag{12}$$

where, $E1$ is the observation error of X_1, Z_{11} and Z_{12} are the observation values of X_1 and X_{1e} respectively. $\beta_{11}>0$ and $\beta_{12}>0$ are the observed gain of ESO, $\alpha>0$and$\delta>0$ are the parameters to be designed.

The function $fal(E_1, \alpha, \delta)$ is defined as

$$fal\left(E_1, \alpha, \delta\right) = \begin{cases} \left|E_1\right|^{\alpha} sgn\left(E_1\right) & \left|E_1\right| > \delta \\ E_1 / \delta^{1-\alpha} & \left|E_1\right| \le \delta \end{cases} \tag{13}$$

By designing a reasonable value of β_{11},β_{12} and α_1, it can be ensured that ESO can observe and dynamically compensate X_1 and X_{1e} well.

Substituting D with the observed variable Z_{12}, equation (10) can be rewritten as

$$U = G^{-1}\begin{bmatrix} c\left(\dot{X}_{1d} - AX_1 - BX_2 - F - Z_{12}\right) + \\ \dot{X}_{2d} + \varepsilon\, sgn\left(s\right) + ks \end{bmatrix} \tag{14}$$

Since the error is less than 1% of the expected distance, the error is bounded and does not affect in the stability of the controller.

3.3 Control Instruction Assignment Design

The control instruction obtained Section 3.1 is acceleration, $U = [a_x, a_y]^T$. However, the actual control variables of the aircraft are the attack angle and the bank angle, so, it is also necessary to obtain the relationship between acceleration and angle.

According to equation (1), (2) and (5), there is

$$\begin{cases} a_x = \dot{v} = -\dfrac{qS}{m} C_D - g\sin\theta \\ a_y = v\dot{\theta} = \dfrac{qS}{m} C_L \cos\sigma - g\cos\theta + \dfrac{v^2\cos\theta}{r} \end{cases} \tag{15}$$

where, $(C_D、\ C_L) = f(\alpha,\ Ma)$. It can be seen that the control variables a_x has a direct mapping relationship with the attack angle, which can be obtained by aerodynamic inverse interpolation. However, the attack angle and the bank angle are coupled items, so they cannot be solved directly by a_y. It is necessary to use the angle of attack and a_y to solve the value of the bank angle.

For the sign of the course angle, the classical method adopts the course angle corridor to determine the sign (Ma, 2017). First set the course angle error threshold. When the course angle error exceeds the preset error threshold, change the bank angle sign to make the course angle return to the corridor; when the course angle error does not exceed the error corridor, keep the course angle sign unchanged.

In this paper, based on the idea of the error threshold, the sign change logic of the bank angle is designed to ensure the follower can maintain the relative position in the z-axis direction. At the same time, the error threshold is designed according to the relative position error in the z-axis direction and cruse angle. Take R_1 and R_2 to satisfy $R_{min} < R_1 < R_2 < R_{max}$. There is

$$sgn(\sigma) = \begin{cases} sgn(R - R_{min}) & R < R_1 \\ -sgn(|\psi_f - \psi_l| - \psi_d) & R_1 < R < R_2 \\ sgn(R - R_{max}) & R_2 < R \end{cases} \tag{16}$$

where, ψ_d represents the error threshold. This is to ensure that when the aerodynamic force meets the control requirements, the aircraft will stay away when it is close and close when it is far away, so that the relative position can be kept within the expected distance range. In the relatively centered distance range, try to keep the speed direction consistent with the leader.

4 SIMULATION

The Common Aero Vehicle (CAV) is selected as the simulation object, its aerodynamic model is (CHEN, 2014)

$$\begin{cases} C_L = -0.232 + 2.94\alpha + 0.295e^{-3.025\times10^{-4}v} \\ C_D = 0.024 + 2.38\alpha^2 + 0.406e^{-9.495\times10^{-4}v} \end{cases} \tag{17}$$

The US 1976 atmospheric model is selected as the atmospheric environment, the characteristic area of the aircraft is S = 0.48378m^2, and the mass of the aircraft is m = 907kg. The maximum attack angle is 25°, and the maximum bank angle is ±90°.

The leader adopts a balanced gliding trajectory, with $\dot{\theta} = 0$, satisfying

$$L\cos(\sigma) + \left(v^2 - \frac{1}{r}\right)\frac{\cos\theta}{r} = 0 \tag{18}$$

The bank angle of the leader is always 0°, and the gliding reaches a height of 30km. The heat flow, dynamic pressure and overload constraints during flight are: Q_{max} = 2000Kw/m^2, q_{max} = 500kPa, n_{max} = 15. R_{min}=5km, R_1=8km, R_2=13km, R_{max}=15km. The initial states of the leader, follower 1 and follower 2 are shown in Table 1.

Table 1: The initial state of the leader and followers.

	h/km	$(\lambda、\ \varphi)$/°	v/m·s^{-1}	θ/°	ψ/°
Leader	60	(0、0)	5000	0	0
follower1	65	(0.13、0.01)	5000	0	0.1
follower2	63	(-0.12、-0.01)	5000	0	0.1

The simulation results are as follows.

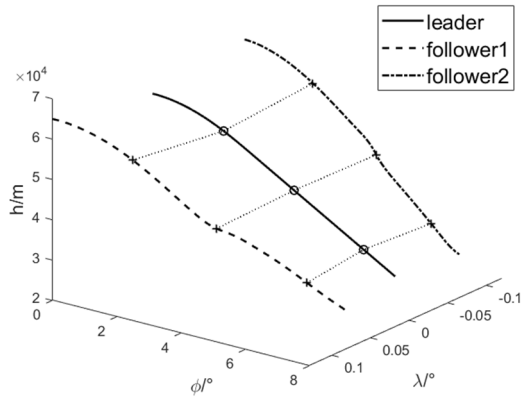

Figure 2: Trajectory of leader and followers.

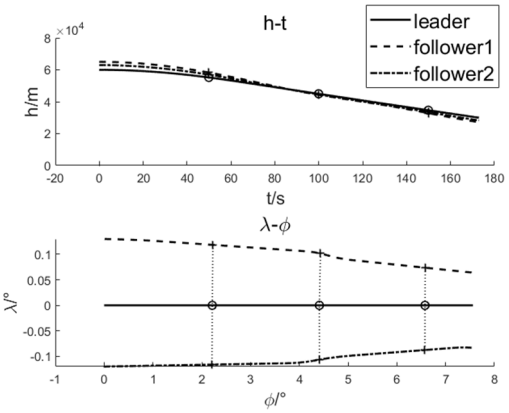

Figure 3: Longitudinal and lateral trajectory.

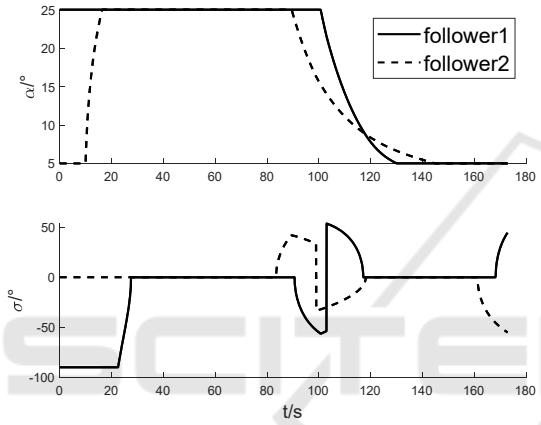

Figure 4: Curves of attack angle and bank angle.

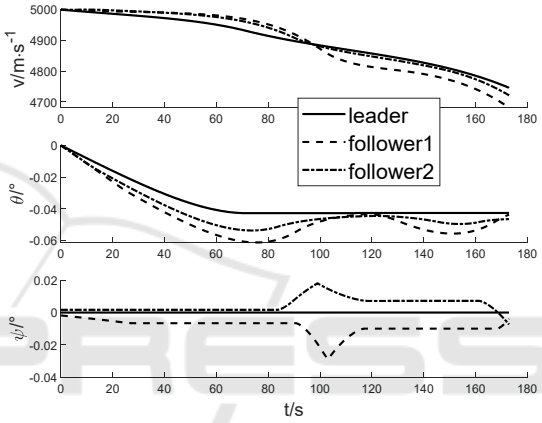

Figure 5: Curves of speed, flight path angle and course angle.

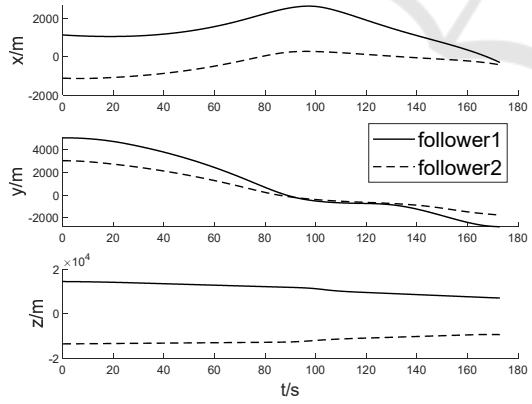

Figure 6: Followers position of x,y and z.

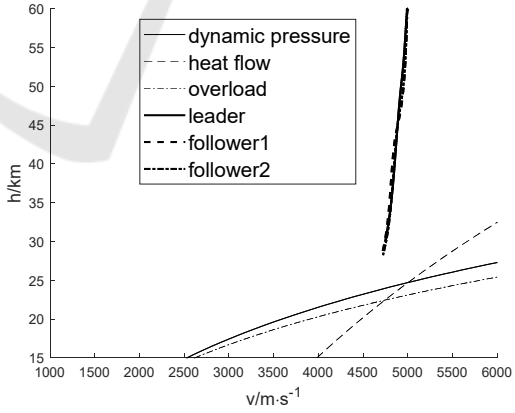

Figure 7: H-V flight corridor.

It can be seen from Figure 2-Figure 7 that the two followers can maintain the spatial configuration: the initial errors in the x-axis direction are 1km and -1km respectively, and with the adjustment during the flight, the errors tend to 0 but are not stable at 0. This is because the limitation of aircraft control capability and the coupling of control variables. During the flight, the error in the x direction of follower1 does not exceed 2km, and that of follower2 does not exceed 1km. Similarly, the initial altitudes of the two followers are 63km and 65km, respectively, and the altitude error (y-direction error) also approaches 0 during the flight, and the steady-state error is not maintained at 0, but the error does not exceed 1.5km.

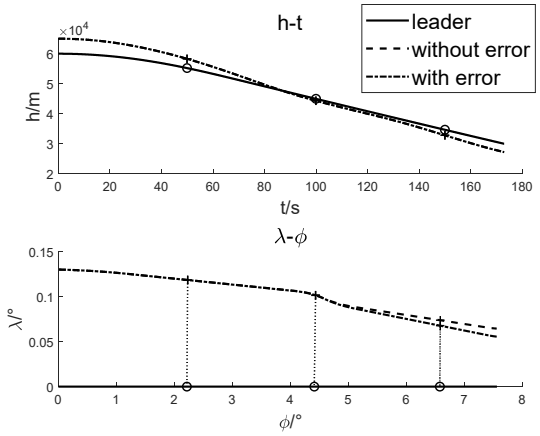

Figure 8: Comparison of trajectories.

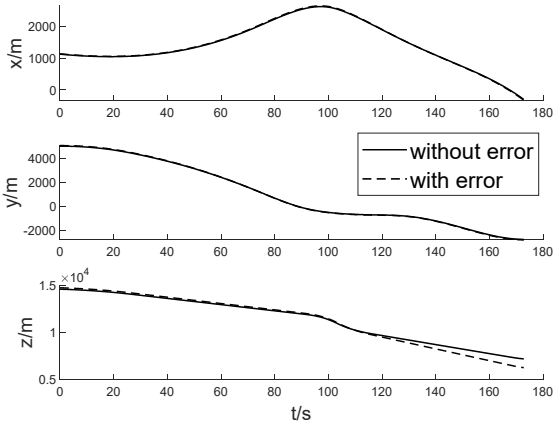

Figure 9: Comparison of position.

In the z direction, the two followers approach the leader after 100s and stabilize at about 8km. In addition, the H-V curves of the leading aircraft are all within the corridor constraints, satisfying the flight process constraints.

Add 1% error to the relative position, and add ESO to the controller at the same time. The observer constants are respectively selected as $\alpha = 0.15$, $\delta = 0.15$, $\beta_1 = 25$, $\beta_2 = 50$. Taking follower1 as the research object, the trajectory simulation comparison results are obtained.

It can be seen from Figure 8 and Figure 9 that after increasing the position error and the observer, the trajectory of follower1 will change. The trajectories have little difference in the x and y directions, but as the flight time increases, the relative position in the z direction gradually develops. This is because the z-direction is expected to have a relatively farther distance, and the error will be larger under the same error ratio. Since the z-direction distance is only controlled by the sign of the bank angle, the accuracy cannot be guaranteed and thus the deviation will occur. However, the distance between the follower and the leader is still within expectations, and the formation configuration can be considered to meet formation requirements.

5 CONCLUSION

1) The sliding mode formation controller designed in this paper can realize the relative position tracking of the leader aircraft by multiple hypersonic glide vehicles in the "leader-follower" mode;

2) Adding ESO to the controller can reduce the modeling error and make the calculation of the follower's trajectory more accurate;

3) The transformation method of control variables in this paper can realize the mapping of aircraft control variables from acceleration to attack angle and bank angle, so as to keep the relative position of the aircraft within the expected distance and realize formation flight.

CONFLICTS OF INTEREST

There is no conflict of interest.

REFERENCES

ZHAO J. Progress in reentry trajectory planning for hypersonic vehicle. *Journal of Systems Engineering and Electronics*, 2014, 25(4):627-639.

GUO M K. Review on cooperative guidance technology for hypersonic flight vehicle. *Aerospace Technology*, 2022(02):75-84. DOI:10.16338/j.issn.2097-0714.20220615.

SHUI X B. A Formation Control Method of Multiple Hypersonic Missiles. *Tactical Missile Technology*, 2020(05):139-148. DOI:10.16358/j.issn.1009-1300.2020.1.050.

An Kai. Research Progress of Formation-Cooperative Control Methods for Low-Speed and High-Speed Vehicle Systems. *Aero Weaponry*. https://kns.cnki.net/ kcms/detail/41.1228.TJ.20220613.1050.001.html.

WANG X. Time-cooperative entry guidance based on analytical profile. *Acta Aeronautica et Astronautica Sinica*, 2019,40(03):239-250.

CHU H. Improved MPSP Methodbased cooperative re-entry guidance for hypersonic gliding vehicles‖*MATEC Web of Conferences*, 2017.

YU J L. Cooperative guidance strategy for multiple hypersonic gliding vehicles system. *Chinese Journal of Aeronautics*, 2020, 33(3):990-1005.

GAO Y. Improved predictor-corrector guidance method for time-coordination entry. *Journal of Beijing University of Aeronautics and Astronautics*, 1-15[2022-10-11]. DOI:10.13700/j.bh.1001-5965.2022.0530.

ZHANG Z L . Cooperative control method of multi-missile formation under uncontrollable speed. *Journal of Northwestern Polytechnical University*, 2021, 39(2):249-257.

ZHANG M Y. Research on Three-dimensional Guidance Law for Cooperative Attack of Multi-unpowered Missiles. *Journal of Projectiles, Rockets, Missiles and Guidance,* 2021, 41(06):1-6. DOI:10.15892/j.cnki.djzdxb.2021.06.001.

WEI S H. Research on a New Multi-missile Formation Co ntroller Design Method. *Journal of Projectiles, Rocke ts, Missiles and Guidance*, 2022,42(03): 69-73. DOI:10.15892/j.cnki.djzdxb.2022.03.014.

Wei Li. Distributed formation control of multiple flight vehicles with considering communication delay. *The 12th International Conference on Mechanical and Aerospace Engineering*, 2021.

Zhao Q, Dong X, Liang Z, et al. Distributed Cooperative Guidance for Multiple Missiles with Fixed and Switching Communication Topologies. *Chinese Journal of Aeronautics*, 2017, 30(4):1761570-1581.

LI W. Research on Time-cooperative Guidance of Multiple Flight Vehicles with Time-varying Velocity. *Acta Armamentarii*, 2020, 41(6):1096-1110.

WANG Z Y. Research on Cooperative Guidance and Formation Flight with Multiple Constraints. *Beijing: Beijing Institute of Technology*, 2018:155-158.

Lu P. Entry guidance: a unified method. Journal of Guidance, Control, and Dynamics, 2014, 37(3):713-728.

Amer Al-Radaideh. Relative Dynamics Modeling and Three-Dimensional Formation Control for Leader-Follower UAVs in the Presence of Wind. AIAA 2020-0878. *AIAA Scitech 2020 Forum*. January 2020.

Brian Coulter. Hypersonic Trajectory Optimization with High-Fidelity Aerothermodynamic Models. AIAA 2021-0715. *AIAA Scitech 2021 Forum*. January 2021.

Wang Z B , Michael J. Grant. Autonomous Entry Guidance for Hypersonic Vehicles by Convex Optimization. *Journal of Spacecraft and Rockets,* 2018, 55:4,993-1006

Wang Z P. Hypersonic Skipping Trajectory Planning for High L/D Gliding Vehicles. AIAA 2017-2135. *21st AIAA International Space Planes and Hypersonics Technologies Conference*. March 2017.

LI M Y. Research on Cooperative Distribution and Strike Strategy of Multi-aircraft to Multi-target. *Beijing: Beijing Institute of Technology*, 2021, 37-45.

Li S C. Profile Tracking Guidance Law Based on Sliding Mode Control. *Acta Aeronautica et Astronautica Sinica*, 2005, 10-25.

Ma Z. Research on the attitude control of quad-rotor UAV based on active disturbance rejection control. *2017 3rd IEEE International Conference on Control Science and Systems Engineering (ICCSSE)*, 2017, pp. 45-49. doi: 10.1109/CCSSE.2017.8087892.

CHEN K J. Launch Vehicle Flight Dynamics and Guidance. *Beijing: National Defense Industry Press*, 2014, 319-320.

WANG G L. Predictor-corrector Reentry Guidance for Hypersonic Vehicles. *Harbin: Harbin Institute of Technology*, 2010, 22-31.